Available online at www.sciencedirect.com
SCIENCE DIRECT®
Journal of Nuclear Materials 352 (2006) 97–106
journal of nuclear materials
www.elsevier.com/locate/jnucmat

Assessment of the constitutive law by inverse methodology: Small punch test and hardness

J. Isselin [a,1], A. Iost [a,*], J. Golek [a], D. Najjar [a], M. Bigerelle [a,b]

[a] *Laboratoire de Métallurgie Physique et Génie des Matériaux, CNRS UMR 8517, Equipe Caractérisation et Propriétés des Périsurfaces, ENSAM, 8 Boulevard Louis XIV, 59046 Lille cedex, France*
[b] *Laboratoire Roberval, FRE CNRS 2833, UTC Centre de Recherches de Royallieu BP 20529, 60205 Compiègne, France*

Abstract

The relevance of small-punch tests and indentation (hardness) tests are compared with regard to the determination of a constitutive law in the case of non active ferrite–bainite steel taken from a French power plant. Firstly, small-punch tests were performed on material samples and the load deflection curves were compared with finite element calculations using the FORGE2 Standard code. As a result the strength coefficient and the strain hardening exponent of Hollomon's constitutive law were determined by an inverse method (Simplex method). Besides, it was shown that a three-parameter constitutive law such as Ludwik Hollomon's leads to an indetermination since its parameters are correlated with each other. Secondly indentation tests were performed with a ball indenter and the parameters of the constitutive law were determined from the analysis of the load–indentation depth curves. Both methods give results in good agreement with the true stress–true strain curve obtained by classical tensile testing, thus proving their applicability to nuclear materials.

1. Introduction

Because of the desire to increase the exploitation lifetime of nuclear plants, the degradation of the components' mechanical properties requires careful attention and monitoring over time. Unfortunately, there is a natural decrease in the available samples which were placed in situ earlier. Under these conditions, small-scale specimen techniques and non-destructive tests become thus more and more attractive in order to characterize the mechanical properties and the in-service degradation of the components.

Among these techniques, the small-punch test and the indentation test allow information to be obtained while using only a very small quantity of material. Initially the small-punch test was developed to study irradiation effects [1]. This test was used to evaluate the ductile to brittle transition temperature (DBTT) [2,3], but also yield stress, ultimate tensile stress [4,5], fracture toughness [6,7] and creep behavior [8,9]. Among the indentation tests, the instrumented tests, which enable to dissociate elastic

* Corresponding author. Tel.: +33 3 20 62 22 33; fax: +33 3 20 62 29 57.
E-mail address: alain.iost@lille.ensam.fr (A. Iost).
[1] Present address: Fracture and Reliability Research Institute, Tohoku University, Aoba 01, Aramaki, Aoba-ku, Sendai 980-8579, Japan.

0022-3115/$ - see front matter © 2006 Elsevier B.V. All rights reserved.
doi:10.1016/j.jnucmat.2006.02.076

behavior from plastic behavior, are the most useful to obtain intrinsic characteristics other than the resistance to penetration. For instance, the ABI (automated ball indentation) method [10] can also be used for the estimation of DBTT and fracture toughness.

The aim of the present investigation is to compare the relevance of indentation and small-punch tests with regard to the determination of a tensile constitutive law for a nuclear material.

2. Experimental procedure

2.1. Materials

This study focuses on a low alloyed steel 15 Mn Mo V (US denomination: A508) taken from a piece of a steam vessel of the power plant located in Montereau (France) after exposure for 145000 h at a temperature of 613 K and a pressure of 130 bar. The microstructure of this alloy, which is presented in Fig. 1, consists of banded ferrite and bainite known as ghost lines resulting from the segregation of the alloying elements and impurities. The grain size is very heterogeneous particularly in the case of the bainite phase.

For the different mechanical tests performed in this investigation, the behavior of the material was assessed in the three usual orientations L (long), T (transverse), S (short-transverse) shown in Fig. 1.

2.2. Tensile tests

Tensile tests have been carried out on 4 mm diameter and 10 mm gauge length specimens with a hydraulic testing machine at a nominal strain rate of $8.32 \times 10^{-3}\ s^{-1}$. The strain hardening exponent n and the strength coefficient k have been calculated from the stress (σ)–strain (ε) curve according to the guidelines of the ISO 10275 standard considering Hollomon's constitutive law

$$\sigma = k\varepsilon^n. \quad (1)$$

2.3. Small-punch tests

2.3.1. Sample preparation

Firstly, specimens have been machined from the piece of vessel by Electro discharge machining to obtain rough discs of 9 mm in diameter and 0.7 mm in thickness. Secondly, the two sides of these discs have been polished with a 1200 paper grade up to a final thickness of 0.5 mm ± 10 μm. Finally, the samples have been electro-polished in a perchloric and acetic acid solution. It is well known that using small specimens for mechanical testing can induce a scattering in the data due to a large size of micro structural constituents relative to the size of the sample. However, in the present investigation, it must be mentioned that the thickness of the overall samples tested was larger than the diameter of 10 grains.

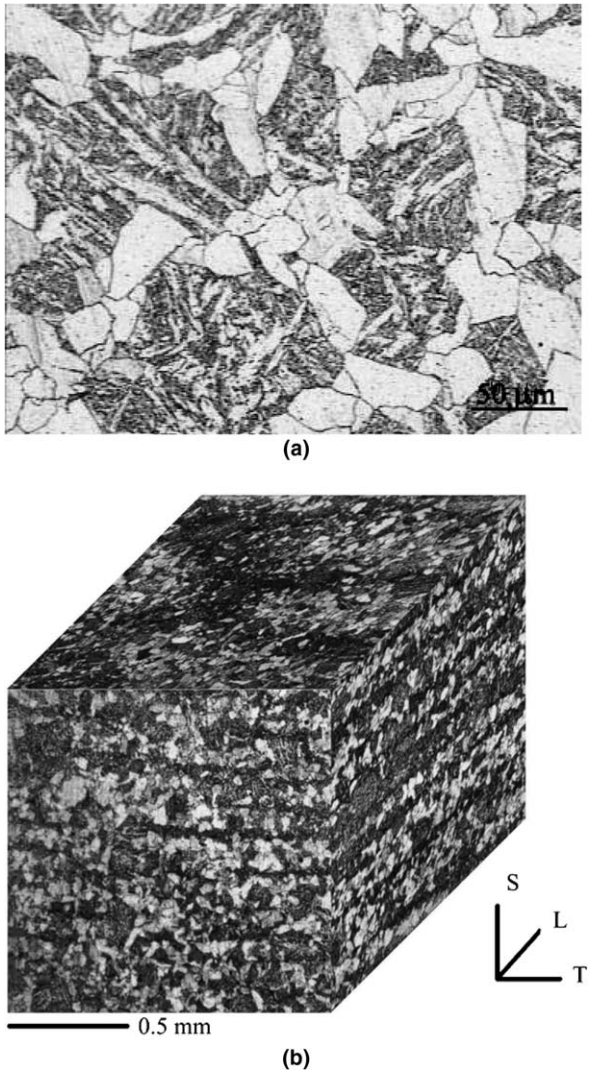

Fig. 1. (a) Microstructure of the low alloyed steel A508 revealed by a Stead le Chatelier solution and (b) the banded structure.

2.3.2. Mechanical testing

The small-punch tests have been carried out with a low speed tensile test machine. The experimental device includes the disc specimen, a 2.5 mm diameter ball and a specimen holder. The specimen holder

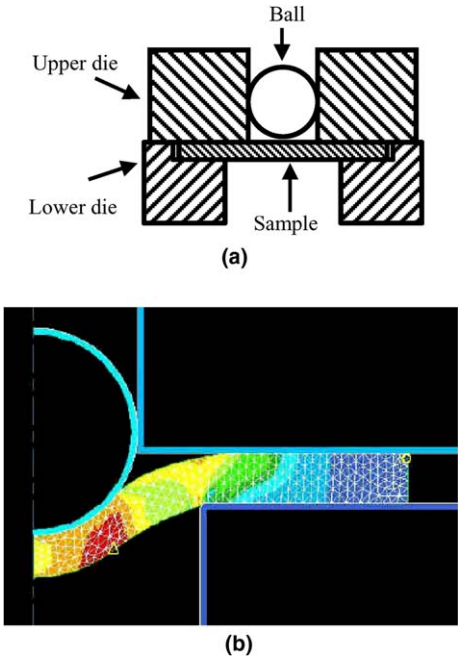

Fig. 2. (a) Schematic representation of the small-punch test jig and (b) of the FORGE2 configuration for simulation without clamping.

consists of an upper die and a lower die on which the sample is placed and centered on a 4 mm diameter hole (the round billet hole edge radius is null). The first function is to clamp the sample with four screws and to lead tanks with a 2.5 mm in diameter hole. A schematic diagram of the test jig is shown in Fig. 2(a).

In this study, small-punch tests have been performed without lubrication at a crosshead speed of 0.1 mm/min and recording simultaneously over time the values of the load and the crosshead displacement.

2.3.3. Finite element modeling

A small-punch test modeling has been developed using the FORGE2 standard code software (Fig. 2(b)). This software has been selected because of an easy communication with the Inverse Method program we developed for the treatment of the experimental data. In the simulation, the upper die, the lower die and the ball have been considered as rigid bodies and the sample has been meshed with 1500 nodes. During the deformation, the upper and lower dies have simply been fixed without applying any force on them. The friction coefficient between the sample and the tools, the Young modulus, the Poisson ratio of the sample and the tools, and the temperature have been fixed at values that equal 0.05, 210 000 MPa, 0.3 and 293 K, respectively.

2.4. Hardness tests

Hardness measurements have been performed by means of a Zwick Z2.5 universal test machine equipped with hardness measurement head and ball indenters with 1.25, 5 or 10 mm diameters (D). The applied load (F) varies from 50 to 1500 N and the curve load–indentation depth is recorded (Fig. 3(a)).

The plastic indentation diameter cannot immediately be derived from the indentation depth because of the existence of material pile-up near the indentation print. Consequently the plastic indentation

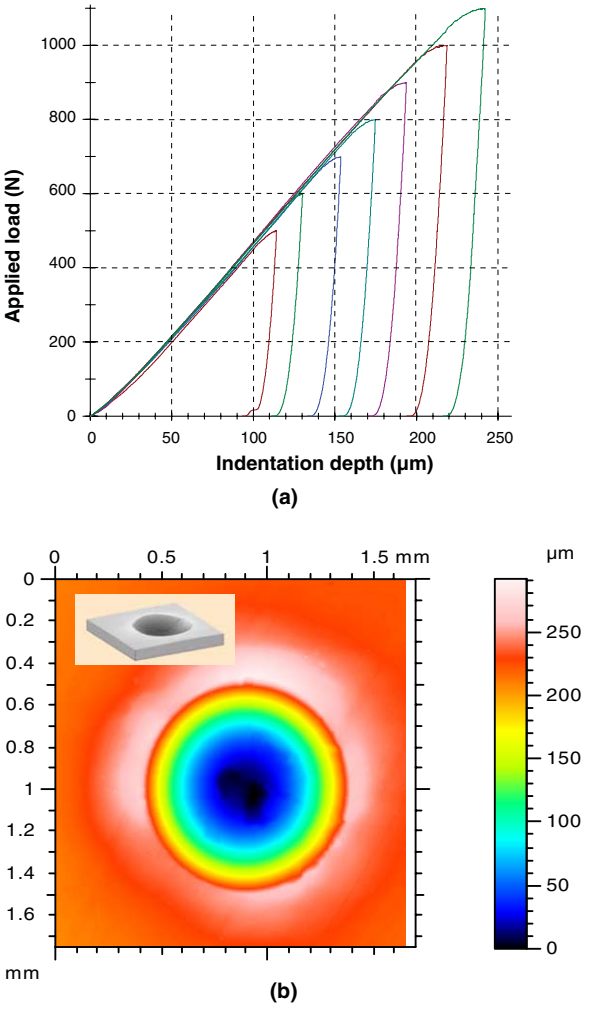

Fig. 3. (a) Examples of load versus displacement curves obtained and (b) example of recorded indentation profile used to determine the plastic indentation diameter.

diameter has been determined from roughness measurements performed with a contacting profilometer KLA Tencor P10 (Fig. 3(b)).

On the one hand, the true plastic strain ε_p associated with the spherical indentation is calculated with the Tabor [11] relation

$$\varepsilon_p = 0.2\frac{d_p}{D}, \tag{2}$$

where d_p is the plastic indentation diameter.

On the other hand, the true stress σ_p is calculated according to the ABI method [12]:

$$\sigma_p = \frac{4F}{\pi d_p^2 \delta} \tag{3}$$

with

$$\delta = \begin{cases} 1.12 & \varphi \leqslant 1, \\ 1.12 + 0.53\ln\varphi & 1 \leqslant \varphi \leqslant 27, \ \varphi = \frac{\varepsilon_p E_{ind}}{0.43\sigma_p}, \\ \delta_{max} = 2.87 & \varphi \geqslant 27, \end{cases} \tag{4}$$

where E_{ind} is the elastic modulus of the indenter and δ is a parameter whose value depends on the stage of development of the plastic zone beneath the indenter [13].

The plastic strains and the plastic stresses for ball indentations are used to plot the homogeneous plastic flow portion of the tensile stress–strain curve with the assumption of a power-law relationship (Eq. (1)).

3. Results and discussion

3.1. Tensile tests

The true stress–true strain curves of the low alloyed steel under study are presented in Fig. 4 for the different orientations and for samples taken either at the skin or in the core of the piece of vessel (with stress strain correlations by ball indentation with various indentation radii obtained in Section 3.3). In the homogeneous plastic deformation domain, which is the domain of interest with regard to the determination of the parameters of the constitutive law of Hollomon, the figure shows that all the curves are very similar meaning that there is no significant influence on the results of the orientation and the location of the samples relatively to the piece of vessel. The values obtained are $k = 1067$ MPa and $n = 0.22$.

3.2. Small punch tests

3.2.1. Mechanical behavior

The load–displacement curves obtained at room temperature for the three orientations are shown in Fig. 5. As for the tensile tests, it can be concluded that there is no influence of the orientation on the results since the curves are really similar. Moreover, the shape of the curves is typical for this kind of test [5]. Indeed, four stages of stress state can be noticed on these curves. The first stage corresponds to the

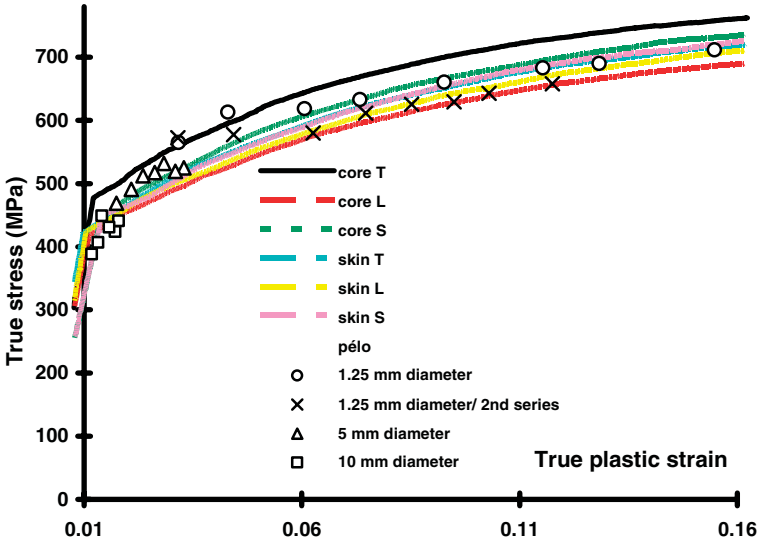

Fig. 4. True stress–true strain tensile curves obtained for the different orientations and sampling locations (core, inner and outer skin of the piece of vessel) and the stress–strain correlations obtained by ball indentation testing with various indenter radii.

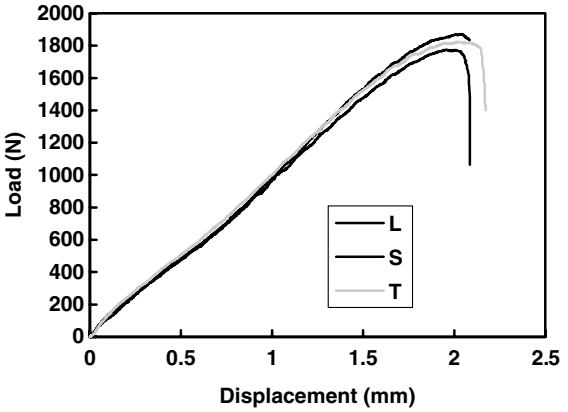

Fig. 5. Influence of the sample orientation on experimental small punch test load–displacement curve (0.5 mm thickness samples tested at room temperature).

elastic bending and ranges from 0 to around 0.25 mm in displacement. During this stage, while the entire sample undergoes an elastic deformation, the ball-sample contact area, which is very small in size, is deformed plastically. The second stage corresponds to the plastic bending state and ranges from 0.25 to around 0.75 mm in displacement. During this stage, the sample plasticized volume progressively increases spreading from the ball-sample contact area in the center of the sample through the overall thickness and in radial direction. Usually, the transition between the second and the third stage is marked by the existence of an inflection point on the curve. In our case, this transition is very slight and is around 0.75 mm in displacement. This third stage corresponds to the membrane stretching and ranges from around 0.75 to 2 mm in displacement. At this stage, the deformation of the sample is not caused by a bending stress but by a stretching stress around the contact area between the ball and the sample. Finally, the fourth stage located from the maximum load to the drop load corresponding to the propagation of the main crack, is the plastic instability area. After the description of these four stages, it is important to keep in mind that, in reality, there are no clear boundary between the different stages from a physical point of view; one stress state simply becomes predominant compared to another one. For instance, the stretching deformation already exists at the beginning of the test, but it becomes only predominant during the membrane stretching stage.

The micrograph in Fig. 6(a) shows a typical overview of a sample tested at room temperature. As expected, the main fracture path is circular. In fact, as described above, the main stressed area just before the fracture is the area around the contact surface between the ball and the sample. Consequently, it is absolutely normal to find the fracture at this particular place. The micrograph in Fig. 6(b) is a high magnification of the fracture surface of the sample which shows many microvoids typical of a ductile fracture.

Fig. 7 shows the influence of the thickness of the samples on the results. As expected, it can be noticed in Fig. 7(a) that the energy (which corresponds to the surface under the load–displacement curve) increases with the thickness of the sample.

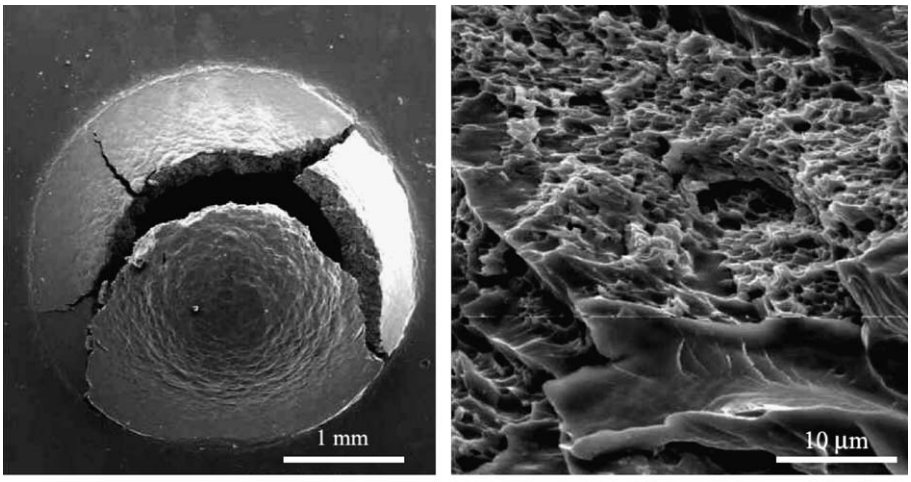

Fig. 6. SEM micrographs: crack shape (a), and fracture surface (b) for 0.5 mm thickness samples tested at room temperature.

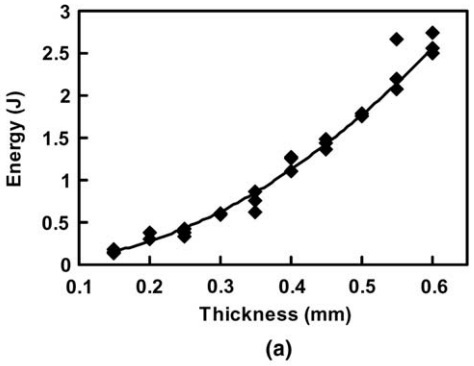

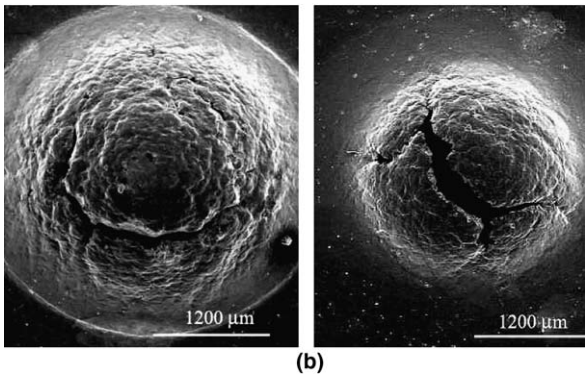

Fig. 7. (a) Influence of the thickness of the sample on the energy value calculated from a small-punch test curve and (b) example of fractured samples having a 0.6 mm thickness (left view) and 0.15 mm thickness (right view).

Two micrographs of fractured samples having a 0.6 and 0.15 mm thickness respectively are presented in Fig. 7(b). In the case of the thicker sample (left view), the main fracture occurs as already described for a sample of 0.5 mm thickness; i.e. in the circular area around the contact surface between the ball and the sample. On the contrary, the main fracture is located at the center of the sample in the case of the thinner sample (right view). This means that, in comparison with the thicker fractured sample, the stress distribution is different. Indeed, in the case of a thick sample, the contact surface between the ball and the sample increases during the test, which causes an increase in both the load and the contact pressure. Because of this pressure, there is rubbing without sliding between the ball and the sample, therefore the main stress at the center of the sample is related to bending but not stretching which is prevented by the rubbing. However if the thickness of the sample is too small, then the contact pressure between the sample and the ball is not sufficient to prevent sliding and the propagation of membrane stretching. This means that the center of the thinner sample simultaneously undergoes a bending and stretching stress explaining why the fracture occurs in this area. The influence of different experimental conditions such as clamping, ball diameter, sample thickness, friction coefficient and rate of deformation were also studied by means of the finite element method and compared with the experimental results [14]. As was shown earlier [15,16] it must be emphasized that friction has a negligible influence on the initial part of the loading, but for the last stage the effect becomes more pronounced.

3.2.2. Analyses of the results by an inverse method

Whatever the inverse method under consideration, a preliminary basic requirement is to define a loss function that measures the accuracy of a model with respect to the experimental data. In this study, we have retained the sum of squared errors to measure the accuracy between points of a load–displacement curve obtained by finite element modeling (FEM) and points of one of the experimental punch test load–displacement curves obtained above. For the FEM, we have initially assumed that the material under consideration obeys the two parameters of Hollomon's constitutive law (Eq. (1)).

The aim of the inverse method is to find the parameters of the selected constitutive law that will minimize the loss function. From all the numerous traditional methods that can be used for the minimization, we have computed the simplex one [17,18] that does not require a gradient estimation which may lead to some numerical problems. From a technical point of view, the first stage of this method consists in defining a square grid of parameters and calculating the value of the loss function for each point of this grid. The minimal value obtained is retained to run our simplex algorithm ($k = 900$ MPa, and $n = 0.18$, see Fig. 8). After optimization, i.e. reduction size of the simplex, the following parameters $k = 975$ and $n = 0.225$ have been found. These values tally with those estimated from the experimental tensile curve with an error lower than 10 % and 3% for k and n, respectively. Such a good accuracy shows that both the selected constitutive law and the selected mesh for the finite element modeling were well adapted to simulate the small-punch test and the numerical methods used in the simulation were well posed.

While the Hollomon's two-parameter law leads to satisfying results in this investigation, it must be mentioned that the Ludwik Hollomon's three-

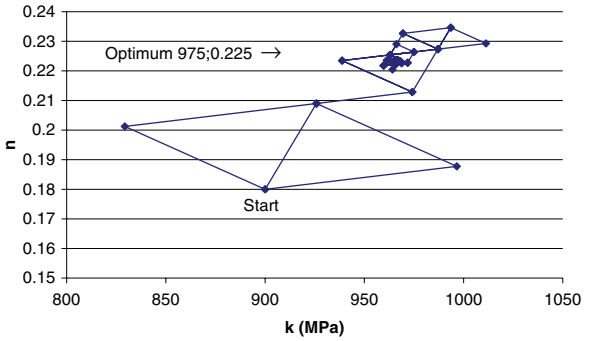

Fig. 8. Illustration of the different steps of the simplex optimization obtained by applying our algorithm to determine the optimal parameters of the Hollomon constitutive law with respect to a FEM of a small-punch test.

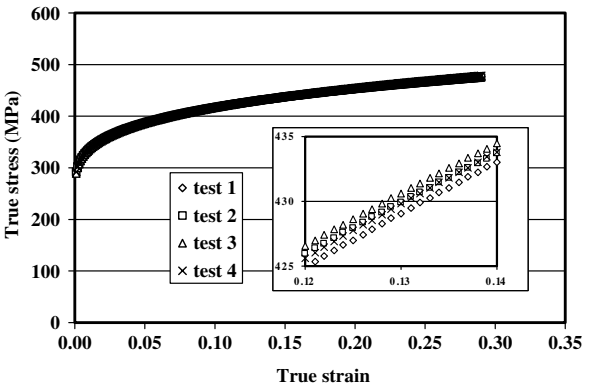

Fig. 9. Effect of a Gaussian random noise on a theoretical tensile curve simulated using the parameters $K = 250$, $a = 1.3$ and $m = 0.29$. The result is illustrated for different perturbed theoretical tensile curves. For the sake of clarity, only four curves out of 10 000 are plotted.

parameter law is also often retained to model the homogeneous plastic domain of a tensile curve

$$\sigma = K(1 + a\varepsilon_{\mathrm{p}}^{m}). \tag{5}$$

However, when considering this three-parameter constitutive law to simulate our punch test by FEM, the following results have been found after simplex optimizations run from two different starting points: ($K = 167$; $a = 1.697$; $m = 0.45$) for the first starting point and ($K = 151$; $a = 1.92$; $m = 0.17$) for the second while the loss function error is near the null value in both cases. In other words, there is not a unique optimal set of values and the final solution depends on the simplex procedure when considering the Ludwik Hollomon's three-parameter constitutive law. It is worth noting that this poor robustness in estimation of the parameters does not result from a non adapted constitutive law relatively to the triaxial stress state of the punch test while Ludwik Hollomon's law normally refers to the uniaxial stress state of a tensile test. In fact, this poor robustness in estimation results from underlying correlations existing between the coefficients of the Ludwik Hollomon's three-parameter constitutive law that may lead to large variability in their estimation irrespective of the nature of the mechanical test. To illustrate this fact, points corresponding to the homogeneous plastic domain of a theoretical tensile curve $(\sigma, \varepsilon_{\mathrm{p}})$ have been simulated using the following values $K = 250$; $a = 1.3$ and $m = 0.29$. Then, a perturbation simulating a plausible experimental error has been introduced by adding a Gaussian random noise with 0 as mean and 5 MPa as standard deviation of the value of the theoretical stress related to each point. Such a procedure has been repeated 10 000 times to simulate 10 000 perturbed theoretical tensile curves. Examples of some of these simulated curves are shown in Fig. 9.

For each curve, the coefficients (a, K, m) of Ludwik Hollomon's law and the coefficients of the simple Hollomon law (n, k) have been determined and reported in Fig. 10. This figure clearly shows firstly that all the coefficients are highly correlated. Secondly, it can be seen that, if the variation range is small (0.283–0.296) for the exponent n related to Hollomon's law, it is considerably larger for the exponent m related to Ludwik Hollomon's law (0.19–0.42). Similar conclusions can be drawn about the strength coefficients of these laws. Besides, in the case of Ludwik Hollomon's law, the product Ka is found to be nearly constant for all the simulations considered.

Moreover, it must be mentioned that even the simple application of our simplex algorithm on the initial theoretical tensile curve $(\sigma, \varepsilon_{\mathrm{p}})$ simulated by FEM (i.e. without any perturbation simulating an experimental error) leads to a large error on the estimation of the value of exponent m. Indeed, the following solution was found: $K = 262$; $a = 1.23$ and $m = 0.22$; values that are not really absurd from a physical point of view but corresponding to an error of 24% for the exponent m. Besides, the loss function is near the null value meaning that the efficiency of our simplex algorithm could not be questioned to explain this result. As time increment, mesh and type of element are identical to those used to simulate the original curve; this variability observed on the estimation of the parameters is only due to a second

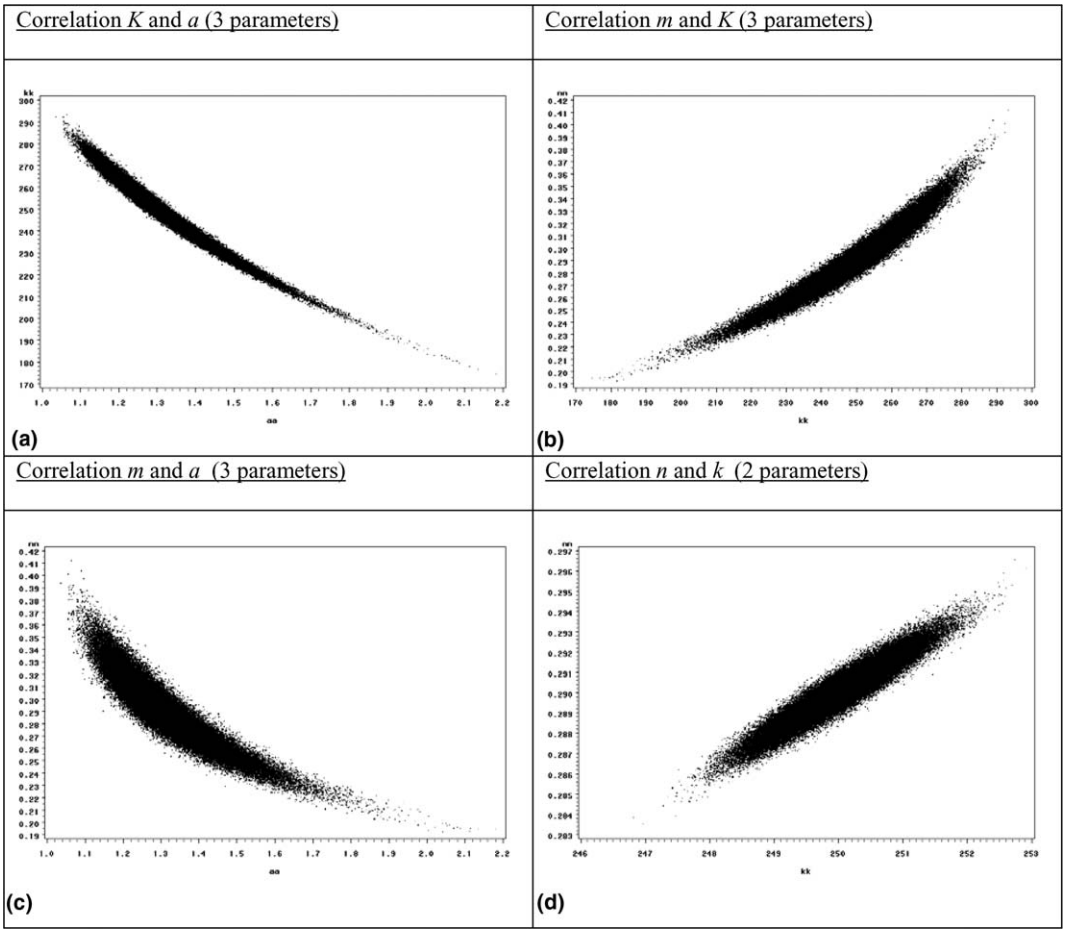

Fig. 10. Correlations existing between the different parameters estimated by the SAS software for the 10 000 perturbed theoretical curves: (a)–(c) correspond to correlations between the three parameters related to Ludwik Hollomon's law while (d) corresponds to the correlation between the two parameters of Hollomon's law.

order numerical error. This physically simply means that even a small perturbation really under the experimental error could lead to high variations on the estimation of the parameters of Ludwik Hollomon's constitutive law. Such limits illustrated from the analysis of simulated tensile curves explain why the Ludwik Hollomon's three-parameter constitutive law is not reliable to model the mechanical behaviour of the material during the simulation of a small-punch test. In fact, for the two simulations of punch tests we already analysed by selecting two different starting points for running the simplex optimisation, we found $Ka = 167 \times .697 = 283$ in the first case and $151 \times 1.92 = 290$ in the second case. These quite similar values indicate that a real correlation exists between these parameters. Different sets of parameters (a, K, m) may correspond to different curves which cannot be visually differentiated (Fig. 9). Consequently, it is impossible to decorrelate the coefficients of Ludwik Hollomon's law from a unique loading curve and using a simple identification based on the small-punch test curves; a two-parameter constitutive law like Hollomon's law should be preferred.

3.3. Hardness tests

Many attempts were made to correlate Vickers or ball indentation with the tensile stress–strain curve. However this subject is still open to discussion. In this paper we used the ABI method described by Haggag et al. [12], but we are aware that the equations are empirical. As reported earlier by Chaudhri [13,19] both radial flow and plasticity theory for rigid-plastic material are inconsistent with experimental data and strain hardening distribution

around indentation is not well established yet. This method must therefore be used with precaution and the results compared with those established by using other methods.

The data (applied load–plastic indentation diameter) obtained from ball hardness indentation are used to plot the plastic stress–strain tensile relationship for a power-law dependence hypotheses. Fig. 4 shows a good correlation between the data obtained with the three different ball diameters (symbols) and the tensile curves plotted for samples with different orientations. From the ball indentation data a strain hardening exponent and a yield strength respectively near 0.22 and 450 MPa ($k = 1145$ MPa) are obtained from the ABI stress–strain curve. These results tally very well with those obtained by the tensile test. These experiments could be performed for post-irradiation characterization studies (as for the punch test) but also in situ, in active environment.

Furthermore, the hardness test seems the most convenient one for studying irradiated materials for which hardening differs from inactive material. It was shown [20] that irradiation effects on the stress strain curve may be associated with a complex mode of deformation at the mesoscale where the composite material is composed of strain softening shear bands that are embedded in a strain hardening matrix. Both types of behaviour may be separately assessed by local indentation (on the opposite punch test and stress–strain curve give only the global response). Other information can also be provided by the observation of the pile-up geometry near the indentation print that is related to residual stress and strain hardening [21–23]. A criticism we would raise concerns the difficulty in observing such geometry in active environment, but pile-up height can be calculated from the variation of hardness with the reciprocal depth of the indentation print [24] with the assumption that the piled-up region also supports the indenter's load and that the normal pressure is distributed uniformly over the projected area of the indentation [25].

4. Conclusions

The use of small-scale specimens associated with an inverse methodology for determining the mechanical properties of irradiated materials is actually an approach of major interest for two main reasons: it reduces as much as possible the irradiation undergone by the staff and it entails a less destructive test. However, the ability of inverse methods to evaluate the mechanical properties of materials is often subjected to caution and the results obtained for a given material must be compared with conventional experiments.

In this study we used the small-punch test and the ball hardness test to estimate the uniaxial yield stress and the hardening exponent of 15 Mn Mo V steel with a banded ferrite–bainite structure provided from a steam vessel of the power plant of Montereau. Both methods give a very good correlation with the results obtained with the conventional tensile test provided a two-parameter constitutive law is used. Conversely we show that a three-parameter law such as Ludwik Hollomon's gives inconsistent results since its three parameters are correlated with each other. The hardness method, after validation for the non active material under study by comparison with the tensile test, is the least destructive to determine in situ the constitutive law of irradiated materials and would be the one of choice for assessing degrading properties in nuclear environment while sacrificing as little as material as possible for trial test.

Acknowledgements

Authors thank EDF for the financial support of this work. In particular, great thanks are due to J.-M. Frund (EDF) for fruitful discussions, and for Véronique Hague for her assistance in English.

References

[1] T. Misawa, H. Sugawara, R. Miura, Y. Hamaguchi, J. Nucl. Mater. 133&134 (1985) 313.
[2] J.M. Baik, J. Kameda, O. Buck, Scripta Metal. 17 (1983) 1443.
[3] J. Kameda, O. Buck, Mater. Sci. Eng. 83 (1986) 29.
[4] G.E. Lucas, A. Okada, M. Kiritani, J. Nucl. Mater. 141–143 (1986) 532.
[5] J.S. Cheon, I.S. Kim, J. Test. Eval. 24 (1996) 255.
[6] X. Mao, H. Takahashi, J. Nucl. Mater 150 (1987) 42.
[7] T. Misawa, S. Nagata, S. Aoki, J. Ishisaka, Y. Hamaguchi, J. Nucl. Mater. 179–181 (1989) 429.
[8] F. Dobes, K. Milicka, J. Test. Eval. 25 (2001) 2481.
[9] S.-I. Komazaki, T. Hashida, T. Shoji, K. Suzuki, J. Test. Eval. 28 (2000) 249.
[10] F.M. Haggag, T.-S. Bryun, J.H. Hong, P.Q. Miraglia, L. Murty, Scripta Mater. 38 (1998) 645.
[11] D. Tabor, The Hardness of Metals, Oxford University, London, UK, 1951.
[12] F.M. Haggag, R.K. Nanstad, D.N. Braski, in: D.L. Marriott, T.R. Mager, W.H. Bamford (Eds.), Innovative approaches to irradiation damage, and fracture analysis,

PVP-vol. 170, The American Society of Mechanical Engineers, p. 101.
[13] M. Chaudhri, Philos. Mag. Lett. 67 (1993) 107.
[14] J. Isselin, Phd thesis, UST Lille, 3273, 2003.
[15] E.N. Campitelli, P. Spätig, R. Bonadé, W. Hoffelner, M. Victoria, J. Nucl. Mater. 335 (2004) 366.
[16] C. Sainte Catherine, J. Messier, C. Poussard, S. Rosinski, J. Foulds, in: Small Specimen Test Technique, in: M.A. Sokolov, J.D. Landes, G.E. Lucas (Eds.), ASTM STP1418, vol. 4, American Society for Testing and Materials, West Conshohoken, PA, 2002, p. 350.
[17] C. Porte, W. Debreuille, A. Delacroix, L'Actualité Chimique (1986) 1.
[18] W. Spendley, G.R. Hext, F.R. Himsworth, Technometrics 4 (1962) 441.
[19] M. Chaudhri, Philos. Mag. A 74 (1996) 1213.
[20] G.R. Odette, M.Y. He, E.G. Donahue, P. Spätig, T. Yamamoto, J. Nucl. Mater. 307–311 (2002) 171.
[21] C. Santos, G.R. Odette, G.E. Lucas, T. Yamamoto, J. Nucl. Mater. 258–263 (1998) 452.
[22] A. Iost, R. Bigot, L. Bourdeau, Matériaux Techniques 12 (1995) 69.
[23] A. Iost, J.B. Vogt, Scripta Mater. 37 (1997) 1499.
[24] A. Iost, R. Bigot, J. Mater. Sci. 31 (1996) 3573.
[25] M. Chaudhri, M. Winter, J. Phys. D: Appl. Phys. 21 (1988) 370.